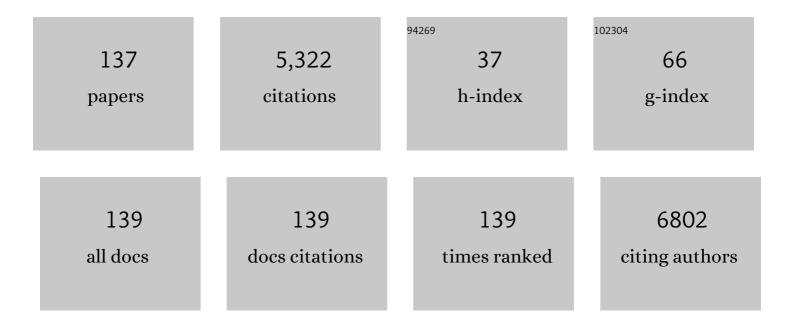
Johnathan W Engle

List of Publications by Year in descending order

Source: https://exaly.com/author-pdf/4023520/publications.pdf Version: 2024-02-01



#	Article	IF	CITATIONS
1	<i>In Vivo</i> Targeting and Imaging of Tumor Vasculature with Radiolabeled, Antibody-Conjugated Nanographene. ACS Nano, 2012, 6, 2361-2370.	7.3	318
2	DNA origami nanostructures can exhibit preferential renal uptake and alleviate acute kidney injury. Nature Biomedical Engineering, 2018, 2, 865-877.	11.6	297
3	Multifunctional unimolecular micelles for cancer-targeted drug delivery and positron emission tomography imaging. Biomaterials, 2012, 33, 3071-3082.	5.7	224
4	Cancer-Targeted Optical Imaging with Fluorescent Zinc Oxide Nanowires. Nano Letters, 2011, 11, 3744-3750.	4.5	199
5	InÂvivo targeting and positron emission tomography imaging of tumor vasculature with 66Ga-labeled nano-graphene. Biomaterials, 2012, 33, 4147-4156.	5.7	197
6	Molybdenum-based nanoclusters act as antioxidants and ameliorate acute kidney injury in mice. Nature Communications, 2018, 9, 5421.	5.8	184
7	Gold Nanorods Conjugated with Doxorubicin and cRGD for Combined Anticancer Drug Delivery and PET Imaging. Theranostics, 2012, 2, 757-768.	4.6	175
8	Ceria Nanoparticles Meet Hepatic Ischemiaâ€Reperfusion Injury: The Perfect Imperfection. Advanced Materials, 2019, 31, e1902956.	11.1	150
9	Magnetic Targeting of Nanotheranostics Enhances Cerenkov Radiation-Induced Photodynamic Therapy. Journal of the American Chemical Society, 2018, 140, 14971-14979.	6.6	148
10	Alpha-Emitters and Targeted Alpha Therapy in Oncology: from Basic Science to Clinical Investigations. Targeted Oncology, 2018, 13, 189-203.	1.7	111
11	A Melaninâ€Based Natural Antioxidant Defense Nanosystem for Theranostic Application in Acute Kidney Injury. Advanced Functional Materials, 2019, 29, 1904833.	7.8	111
12	Positron Emission Tomography Imaging of CD105 Expression with a 64Cu-Labeled Monoclonal Antibody: NOTA Is Superior to DOTA. PLoS ONE, 2011, 6, e28005.	1.1	101
13	Low-dose targeted radionuclide therapy renders immunologically cold tumors responsive to immune checkpoint blockade. Science Translational Medicine, 2021, 13, .	5.8	92
14	Ultra-small iron-gallic acid coordination polymer nanoparticles for chelator-free labeling of ⁶⁴ Cu and multimodal imaging-guided photothermal therapy. Nanoscale, 2017, 9, 12609-12617.	2.8	90
15	Efficient Uptake of ¹⁷⁷ Luâ€Porphyrinâ€PEG Nanocomplexes by Tumor Mitochondria for Multimodalâ€Imagingâ€Guided Combination Therapy. Angewandte Chemie - International Edition, 2018, 57, 218-222.	7.2	85
16	Positron emission tomography imaging of CD105 expression during tumor angiogenesis. European Journal of Nuclear Medicine and Molecular Imaging, 2011, 38, 1335-1343.	3.3	77
17	Chiralityâ€Driven Transportation and Oxidation Prevention by Chiral Selenium Nanoparticles. Angewandte Chemie - International Edition, 2020, 59, 4406-4414.	7.2	77
18	Positron emission tomography imaging of CD105 expression with 89Zr-Df-TRC105. European Journal of Nuclear Medicine and Molecular Imaging, 2012, 39, 138-148.	3.3	75

#	Article	IF	CITATIONS
19	Spectroscopic and computational investigation of actinium coordination chemistry. Nature Communications, 2016, 7, 12312.	5.8	73
20	Renal-Clearable Ultrasmall Coordination Polymer Nanodots for Chelator-Free ⁶⁴ Cu-Labeling and Imaging-Guided Enhanced Radiotherapy of Cancer. ACS Nano, 2017, 11, 9103-9111.	7.3	73
21	Multimodality Imaging of Breast Cancer Experimental Lung Metastasis with Bioluminescence and a Monoclonal Antibody Dual-Labeled with ⁸⁹ Zr and IRDye 800CW. Molecular Pharmaceutics, 2012, 9, 2339-2349.	2.3	63
22	89Zr Radiochemistry for Positron Emission Tomography. Medicinal Chemistry, 2011, 7, 389-394.	0.7	63
23	Intrabilayer ⁶⁴ Cu Labeling of Photoactivatable, Doxorubicin-Loaded Stealth Liposomes. ACS Nano, 2017, 11, 12482-12491.	7.3	62
24	Selfâ€Amplified Photodynamic Therapy through the ¹ O ₂ â€Mediated Internalization of Photosensitizers from a Ppaâ€Bearing Block Copolymer. Angewandte Chemie - International Edition, 2020, 59, 3711-3717.	7.2	62
25	Synthesis and Characterization of the Actinium Aquo Ion. ACS Central Science, 2017, 3, 176-185.	5.3	53
26	Intrathecal Administration of Nanoclusters for Protecting Neurons against Oxidative Stress in Cerebral Ischemia/Reperfusion Injury. ACS Nano, 2019, 13, 13382-13389.	7.3	53
27	Aptamer-Conjugated Framework Nucleic Acids for the Repair of Cerebral Ischemia-Reperfusion Injury. Nano Letters, 2019, 19, 7334-7341.	4.5	51
28	Immuno-PET of Tissue Factor in Pancreatic Cancer. Journal of Nuclear Medicine, 2012, 53, 1748-1754.	2.8	49
29	Openâ€Shell Nanosensitizers for Glutathione Responsive Cancer Sonodynamic Therapy. Advanced Materials, 2022, 34, e2110283.	11.1	48
30	Radiolabeled, Antibody-Conjugated Manganese Oxide Nanoparticles for Tumor Vasculature Targeted Positron Emission Tomography and Magnetic Resonance Imaging. ACS Applied Materials & Interfaces, 2017, 9, 38304-38312.	4.0	47
31	PET radiometals for antibody labeling. Journal of Labelled Compounds and Radiopharmaceuticals, 2018, 61, 636-651.	0.5	43
32	Amyloid duration is associated with preclinical cognitive decline and tau PET. Alzheimer's and Dementia: Diagnosis, Assessment and Disease Monitoring, 2020, 12, e12007.	1.2	43
33	Evaluating the electronic structure of formal Ln ^{II} ions in Ln ^{II} (C ₅ H ₄ SiMe ₃) ₃ 3/sub>3using XANES spectroscopy and DFT calculations. Chemical Science, 2017, 8, 6076-6091.	3.7	42
34	CD146â€Targeted Multimodal Imageâ€Guided Photoimmunotherapy of Melanoma. Advanced Science, 2019, 6, 1801237.	5.6	42
35	Establishing Radiolanthanum Chemistry for Targeted Nuclear Medicine Applications. Chemistry - A European Journal, 2020, 26, 1238-1242.	1.7	42
36	Evaluation of nitrogen-rich macrocyclic ligands for the chelation of therapeutic bismuth radioisotopes. Nuclear Medicine and Biology, 2015, 42, 428-438.	0.3	41

#	Article	IF	CITATIONS
37	Site-Specific Immuno-PET Tracer to Image PD-L1. Molecular Pharmaceutics, 2019, 16, 2028-2036.	2.3	41
38	Positron Emission Tomography and Optical Imaging of Tumor CD105 Expression with a Dual-Labeled Monoclonal Antibody. Molecular Pharmaceutics, 2012, 9, 645-653.	2.3	39
39	Sizeâ€Optimized Ultrasmall Porous Silica Nanoparticles Depict Vasculatureâ€Based Differential Targeting in Triple Negative Breast Cancer. Small, 2019, 15, e1903747.	5.2	39
40	90Y-NM600 targeted radionuclide therapy induces immunologic memory in syngeneic models of T-cell Non-Hodgkin's Lymphoma. Communications Biology, 2019, 2, 79.	2.0	39
41	Positron Emission Tomography Imaging of Tumor Angiogenesis with a ⁶⁶ Ga-Labeled Monoclonal Antibody. Molecular Pharmaceutics, 2012, 9, 1441-1448.	2.3	37
42	The Production of Ac-225. Current Radiopharmaceuticals, 2018, 11, 173-179.	0.3	35
43	A "Missileâ€Ðetonation―Strategy to Precisely Supply and Efficiently Amplify Cerenkov Radiation Energy for Cancer Theranostics. Advanced Materials, 2019, 31, e1904894.	11.1	35
44	Simultaneous Separation of Actinium and Radium Isotopes from a Proton Irradiated Thorium Matrix. Scientific Reports, 2017, 7, 8216.	1.6	34
45	Noninvasive Imaging and Quantification of Radiotherapy-Induced PD-L1 Upregulation with ⁸⁹ Zr–Df–Atezolizumab. Bioconjugate Chemistry, 2019, 30, 1434-1441.	1.8	34
46	Efficient renal clearance of DNA tetrahedron nanoparticles enables quantitative evaluation of kidney function. Nano Research, 2019, 12, 637-642.	5.8	34
47	Temporal analysis of type 1 interferon activation in tumor cells following external beam radiotherapy or targeted radionuclide therapy. Theranostics, 2021, 11, 6120-6137.	4.6	34
48	HPMA-based star polymer biomaterials with tuneable structure and biodegradability tailored for advanced drug delivery to solid tumours. Biomaterials, 2020, 235, 119728.	5.7	33
49	Prevention of Hepatic Ischemia-Reperfusion Injury by Carbohydrate-Derived Nanoantioxidants. Nano Letters, 2020, 20, 6510-6519.	4.5	32
50	In Vivo Tumor-Targeted Dual-Modality PET/Optical Imaging with a Yolk/Shell-Structured Silica Nanosystem. Nano-Micro Letters, 2018, 10, 65.	14.4	31
51	ImmunoPET imaging of CD38 in murine lymphoma models using 89Zr-labeled daratumumab. European Journal of Nuclear Medicine and Molecular Imaging, 2018, 45, 1372-1381.	3.3	30
52	Py-Macrodipa: A Janus Chelator Capable of Binding Medicinally Relevant Rare-Earth Radiometals of Disparate Sizes. Journal of the American Chemical Society, 2021, 143, 10429-10440.	6.6	30
53	Intrinsically Zirconium-89-Labeled Manganese Oxide Nanoparticles for <i>In Vivo</i> Dual-Modality Positron Emission Tomography and Magnetic Resonance Imaging. Journal of Biomedical Nanotechnology, 2018, 14, 900-909.	0.5	29
54	Production and in vivo PET/CT imaging of the theranostic pair 132/135La. Scientific Reports, 2019, 9, 10658.	1.6	29

#	Article	IF	CITATIONS
55	Proton-induced production and radiochemical isolation of 44Ti from scandium metal targets for 44Ti/44Sc generator development. Nuclear Medicine and Biology, 2017, 50, 25-32.	0.3	28
56	¹¹ C-(<i>R</i>)-PK11195 PET Imaging of Microglial Activation and Response to Minocycline in Zymosan-Treated Rats. Journal of Nuclear Medicine, 2011, 52, 257-262.	2.8	27
57	Recommended Nuclear Data for the Production of Selected Therapeutic Radionuclides. Nuclear Data Sheets, 2019, 155, 56-74.	0.7	27
58	Radiolabeled Î ³ -AApeptides: a new class of tracers for positron emission tomography. Chemical Communications, 2012, 48, 7850.	2.2	26
59	Cross sections from proton irradiation of thorium at 800 MeV. Physical Review C, 2013, 88, .	1.1	26
60	Formation cross-sections and chromatographic separation of protactinium isotopes formed in proton-irradiated thorium metal. Radiochimica Acta, 2016, 104, 291-304.	0.5	25
61	Developing the 134Ce and 134La pair as companion positron emission tomography diagnostic isotopes for 225Ac and 227Th radiotherapeutics. Nature Chemistry, 2021, 13, 284-289.	6.6	25
62	Radiometric evaluation of diglycolamide resins for the chromatographic separation of actinium from fission product lanthanides. Talanta, 2017, 175, 318-324.	2.9	24
63	Chromatographic separation of the theranostic radionuclide 111Ag from a proton irradiated thorium matrix. Analytica Chimica Acta, 2018, 998, 75-82.	2.6	24
64	[^{nat/44} Sc(pypa)] ^{â^'} : Thermodynamic Stability, Radiolabeling, and Biodistribution of a Prostate-Specific-Membrane-Antigen-Targeting Conjugate. Inorganic Chemistry, 2020, 59, 1985-1995.	1.9	23
65	Nonuniform Cardiac Denervation Observed by 11C-meta-Hydroxyephedrine PET in 6-OHDA-Treated Monkeys. PLoS ONE, 2012, 7, e35371.	1.1	22
66	Prenatal Stress Induces Increased Striatal Dopamine Transporter Binding in Adult Nonhuman Primates. Biological Psychiatry, 2013, 74, 502-510.	0.7	22
67	Preparation and in vivo characterization of 51MnCl2 as PET tracer of Ca2+ channel-mediated transport. Scientific Reports, 2017, 7, 3033.	1.6	22
68	Simplified and automatable radiochemical separation strategy for the production of radiopharmaceutical quality 86Y using single column extraction chromatography. Applied Radiation and Isotopes, 2018, 142, 28-31.	0.7	22
69	Chiralityâ€Ðriven Transportation and Oxidation Prevention by Chiral Selenium Nanoparticles. Angewandte Chemie, 2020, 132, 4436-4444.	1.6	22
70	Tissue Factorâ€Targeted ImmunoPET Imaging and Radioimmunotherapy of Anaplastic Thyroid Cancer. Advanced Science, 2020, 7, 1903595.	5.6	22
71	Bulk production and evaluation of high specific activity 186gRe for cancer therapy using enriched 186WO3 targets in a proton beam. Nuclear Medicine and Biology, 2017, 49, 24-29.	0.3	21
72	Noninvasive Evaluation of CD20 Expression Using ⁶⁴ Cu-Labeled F(ab′) ₂ Fragments of Obinutuzumab in Lymphoma. Journal of Nuclear Medicine, 2021, 62, 372-378.	2.8	21

#	Article	IF	CITATIONS
73	¹⁷⁷ Lu-NM600 Targeted Radionuclide Therapy Extends Survival in Syngeneic Murine Models of Triple-Negative Breast Cancer. Journal of Nuclear Medicine, 2020, 61, 1187-1194.	2.8	20
74	Intracellular signaling pathway in dendritic cells and antigen transport pathway in vivo mediated by an OVA@DDAB/PLGA nano-vaccine. Journal of Nanobiotechnology, 2021, 19, 394.	4.2	20
75	Nuclear excitation functions of proton-induced reactions (Ep= 35–90 MeV) from Fe, Cu, and Al. Nuclear Instruments & Methods in Physics Research B, 2016, 386, 44-53.	0.6	19
76	Noninvasive Trafficking of Brentuximab Vedotin and PET Imaging of CD30 in Lung Cancer Murine Models. Molecular Pharmaceutics, 2018, 15, 1627-1634.	2.3	19
77	86/90Y-Based Theranostics Targeting Angiogenesis in a Murine Breast Cancer Model. Molecular Pharmaceutics, 2018, 15, 2606-2613.	2.3	19
78	86/90Y-Labeled Monoclonal Antibody Targeting Tissue Factor for Pancreatic Cancer Theranostics. Molecular Pharmaceutics, 2020, 17, 1697-1705.	2.3	19
79	Antibody and fragment-based PET imaging of CTLA-4+ T-cells in humanized mouse models. American Journal of Cancer Research, 2019, 9, 53-63.	1.4	19
80	Cyclotron produced ¹³² La as a PET imaging surrogate of therapeutic ²²⁵ Ac. Journal of Nuclear Medicine, 2021, 62, jnumed.120.255794.	2.8	18
81	ImmunoPET of trophoblast cell-surface antigen 2 (Trop-2) expression in pancreatic cancer. European Journal of Nuclear Medicine and Molecular Imaging, 2022, 49, 861-870.	3.3	18
82	Evaluation of a chloride-based 89Zr isolation strategy using a tributyl phosphate (TBP)-functionalized extraction resin. Nuclear Medicine and Biology, 2018, 64-65, 1-7.	0.3	17
83	Mathematical modeling of positron emission tomography (PET) data to assess radiofluoride transport in living plants following petiolar administration. Plant Methods, 2015, 11, 18.	1.9	16
84	Surfactant-Stripped Pheophytin Micelles for Multimodal Tumor Imaging and Photodynamic Therapy. ACS Applied Bio Materials, 2019, 2, 544-554.	2.3	16
85	ImmunoPET Imaging of CD146 in Murine Models of Intrapulmonary Metastasis of Non-Small Cell Lung Cancer. Molecular Pharmaceutics, 2017, 14, 3239-3247.	2.3	15
86	Excitation functions for (p,x) reactions of niobium in the energy range of Ep = 40–90 MeV. Nuclear Instruments & Methods in Physics Research B, 2018, 429, 53-74.	0.6	15
87	Improved production of 76Br, 77Br and 80mBr via CoSe cyclotron targets and vertical dry distillation. Nuclear Medicine and Biology, 2020, 80-81, 32-36.	0.3	15
88	Development and characterization of CD54-targeted immunoPET imaging in solid tumors. European Journal of Nuclear Medicine and Molecular Imaging, 2020, 47, 2765-2775.	3.3	15
89	ImmunoPET/NIRF/Cerenkov multimodality imaging of ICAM-1 in pancreatic ductal adenocarcinoma. European Journal of Nuclear Medicine and Molecular Imaging, 2021, 48, 2737-2748.	3.3	14
90	Automated, cassette-based isolation and formulation of high-purity [61Cu]CuCl2 from solid Ni targets. EJNMMI Radiopharmacy and Chemistry, 2020, 5, 21.	1.8	14

#	Article	IF	CITATIONS
91	Meitner-Auger Electron Emitters for Targeted Radionuclide Therapy: Mercury-197m/g and Antimony-119 Current Radiopharmaceuticals, 2021, 14, 394-419.	0.3	13
92	Accelerator Production of Scandium Radioisotopes: Sc-43, Sc-44, and Sc-47. Current Radiopharmaceuticals, 2021, 14, 359-373.	0.3	13
93	ImmunoPET of CD146 in Orthotopic and Metastatic Breast Cancer Models. Bioconjugate Chemistry, 2021, 32, 1306-1314.	1.8	13
94	Antioxidant and C5a-blocking strategy for hepatic ischemia–reperfusion injury repair. Journal of Nanobiotechnology, 2021, 19, 107.	4.2	13
95	Production of 34mCl and 38Cl via the (d,Î \pm) reaction on 36Ar and natAr gas at 8.4MeV. Applied Radiation and Isotopes, 2011, 69, 75-79.	0.7	12
96	Large-Scale Production of ^{119m} Te and ¹¹⁹ Sb for Radiopharmaceutical Applications. ACS Central Science, 2019, 5, 494-505.	5.3	12
97	Coordination chemistry of [Y(pypa)] ^{â^`} and comparison immuno-PET imaging of [⁴⁴ Sc]Sc- and [⁸⁶ Y]Y-pypa-phenyl-TRC105. Dalton Transactions, 2020, 49, 5547-5562.	1.6	12
98	ImmunoPET Imaging of TIMâ€3 in Murine Melanoma Models. Advanced Therapeutics, 2020, 3, 200018.	1.6	12
99	Safety and feasibility of an in situ vaccination and immunomodulatory targeted radionuclide combination immuno-radiotherapy approach in a comparative (companion dog) setting. PLoS ONE, 2021, 16, e0255798.	1.1	12
100	64Cu-labeled daratumumab F(ab′)2 fragment enables early visualization of CD38-positive lymphoma. European Journal of Nuclear Medicine and Molecular Imaging, 2022, 49, 1470-1481.	3.3	12
101	Selfâ€Amplified Photodynamic Therapy through the ¹ O ₂ â€Mediated Internalization of Photosensitizers from a Ppaâ€Bearing Block Copolymer. Angewandte Chemie, 2020, 132, 3740-3746.	1.6	11
102	Dual-labeled pertuzumab for multimodality image-guided ovarian tumor resection. American Journal of Cancer Research, 2019, 9, 1454-1468.	1.4	11
103	Efficient Uptake of ¹⁷⁷ Luâ€Porphyrinâ€PEG Nanocomplexes by Tumor Mitochondria for Multimodalâ€Imagingâ€Guided Combination Therapy. Angewandte Chemie, 2018, 130, 224-228.	1.6	10
104	Engineering biocompatible TeSex nano-alloys as a versatile theranostic nanoplatform. National Science Review, 2021, 8, .	4.6	10
105	Production, Purification, and Applications of a Potential Theranostic Pair: Cobalt-55 and Cobalt-58m. Diagnostics, 2021, 11, 1235.	1.3	10
106	HER2-targeted multimodal imaging of anaplastic thyroid cancer. American Journal of Cancer Research, 2019, 9, 2413-2427.	1.4	10
107	Characterization of the radiosynthesis and purification of [18F]THK-5351, a PET ligand for neurofibrillary tau. Applied Radiation and Isotopes, 2017, 130, 230-237.	0.7	9
108	Radiochemical isolation method for the production of 52gMn from natCr for accelerator targets. Applied Radiation and Isotopes, 2019, 146, 99-103.	0.7	9

#	Article	IF	CITATIONS
109	Cross sections of the 36Ar(d,α)34mCl, 40Ar(d,α)38Cl, and 40Ar(d,p)41Ar nuclear reactions below 8.4MeV. Applied Radiation and Isotopes, 2012, 70, 355-359.	0.7	8
110	ImmunoPET imaging of CD38 expression in hepatocellular carcinoma using Cu-labeled daratumumab. American Journal of Translational Research (discontinued), 2019, 11, 6007-6015.	0.0	8
111	ImmunoPET of CD146 in a Murine Hindlimb Ischemia Model. Molecular Pharmaceutics, 2018, 15, 3434-3441.	2.3	7
112	The Unrealized Potential of 34mCl for Radiopharmaceutical Research with PET. Current Radiopharmaceuticals, 2011, 4, 102-108.	0.3	7
113	A review of accelerator-produced Ga-68 with solid targets. Current Radiopharmaceuticals, 2020, 13, 315-324.	0.3	7
114	Nuclear excitation functions from 40 to 200 MeV proton irradiation of terbium. Nuclear Instruments & Methods in Physics Research B, 2016, 366, 206-216.	0.6	6
115	Low-Dose Radiation Potentiates the Propagation of Anti-Tumor Immunity against Melanoma Tumor in the Brain after In Situ Vaccination at a Tumor outside the Brain. Radiation Research, 2021, 195, 522-540.	0.7	6
116	MCNPX characterization of the secondary neutron flux at the Los Alamos Isotope Production Facility. Nuclear Instruments and Methods in Physics Research, Section A: Accelerators, Spectrometers, Detectors and Associated Equipment, 2014, 754, 71-82.	0.7	5
117	Separation of 103Ru from a proton irradiated thorium matrix: A potential source of Auger therapy radionuclide 103mRh. PLoS ONE, 2017, 12, e0190308.	1.1	5
118	Spatiotemporal Distribution of Agrin after Intrathecal Injection and Its Protective Role in Cerebral Ischemia/Reperfusion Injury. Advanced Science, 2020, 7, 1902600.	5.6	5
119	Proton-induced reactions on Fe, Cu, and Ti from threshold to 55 MeV. European Physical Journal A, 2021, 57, 1.	1.0	5
120	A heavy-ion production channel of 149Tb via 63Cu bombardment of 89Y. Applied Radiation and Isotopes, 2021, 178, 109935.	0.7	5
121	Excitation function of 54Fe(p, \hat{l} ±)51Mn from 9.5 MeV to 18 MeV. Nuclear Physics A, 2022, 1021, 122424.	0.6	5
122	Half-life of Mn51. Physical Review C, 2017, 96, .	1.1	4
123	Alternative strategies for the synthesis of [11C]ER176 for PET imaging of neuroinflammation. Applied Radiation and Isotopes, 2021, 178, 109954.	0.7	4
124	PET Measures of D1, D2, and DAT Binding Are Associated With Heightened Tactile Responsivity in Rhesus Macaques: Implications for Sensory Processing Disorder. Frontiers in Integrative Neuroscience, 2019, 13, 29.	1.0	3
125	Characterization of actinide resin for separation of 51,52gMn from bulk target material. Nuclear Medicine and Biology, 2021, 96-97, 19-26.	0.3	3
126	A High Separation Factor for 165Er from Ho for Targeted Radionuclide Therapy. Molecules, 2021, 26, 7513.	1.7	3

#	Article	IF	CITATIONS
127	Radiochlorine: an underutilized halogen tool. Radiochimica Acta, 2019, 107, 1027-1031.	0.5	2
128	Labeling of Erythrocytes by Porphyrinâ€Phospholipid. Advanced NanoBiomed Research, 2021, 1, 2000013.	1.7	2
129	Metal ion size profoundly affects H3glyox chelate chemistry. RSC Advances, 2021, 11, 15663-15674.	1.7	2
130	Frontispiece: Chiralityâ€Driven Transportation and Oxidation Prevention by Chiral Selenium Nanoparticles. Angewandte Chemie - International Edition, 2020, 59, .	7.2	1
131	A Third Generation Potentially Bifunctional Trithiol Chelate, Its nat,1XXSb(III) Complex, and Selective Chelation of Radioantimony (119Sb) from Its Sn Target. Inorganic Chemistry, 2021, 60, 15223-15232.	1.9	1
132	Fluoride transport in Brassica: A positron emission tomography botanical study. , 2011, , .		0
133	Frontispiz: Chiralityâ€Driven Transportation and Oxidation Prevention by Chiral Selenium Nanoparticles. Angewandte Chemie, 2020, 132, .	1.6	Ο
134	Frontispiece: Establishing Radiolanthanum Chemistry for Targeted Nuclear Medicine Applications. Chemistry - A European Journal, 2020, 26, .	1.7	0
135	Status and future perspectives of Meitner-Auger and low energy electron-emitting radionuclides for targeted radionuclide therapy. Nuclear Medicine and Biology, 2021, 94-95, 106.	0.3	Ο
136	ImmunoPET of the differential expression of CD146 in breast cancer. American Journal of Cancer Research, 2021, 11, 1586-1599.	1.4	0
137	Intermetallic cobalt–gallium targets for production of germanium radioisotopes. Applied Radiation and Isotopes, 2022, 187, 110307.	0.7	Ο